Konrad-Zuse-Zentrum für Informationstechnik Berlin

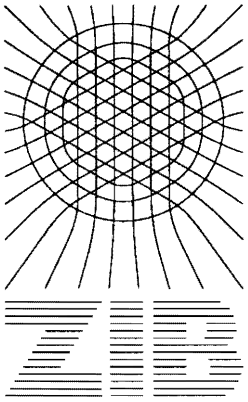

Ulrich H.E. Hansmann Yuko Okamoto

Comparative Study of Multicanonical and Simulated Annealing Algorithms in the Protein Folding Problem

Preprint SC 94–20 (August 1994)

Herausgegeben vom
Konrad-Zuse-Zentrum für Informationstechnik Berlin
Heilbronner Str. 10
D-10711 Berlin-Wilmersdorf
Telefon: 030-89604-0
Telefax: 030-89604-125
e-mail : bibliothek@zib-berlin.de

Umschlagsatz und Druck: Rabe KG Buch- und Offsetdruck Berlin

ISSN 0933-7911

SC-94-
NWU-5/94
July 1994

Comparative Study of Multicanonical and Simulated Annealing Algorithms in the Protein Folding Problem

Ulrich H.E. Hansmann[1] and Yuko Okamoto[2]

[1] *Konrad Zuse Zentrum für Informationstechnik Berlin (ZIB)*
10711 Berlin, Germany

[2] *Department of Physics, Nara Women's University, Nara 630, Japan*

ABSTRACT

We compare a few variants of the recently proposed multicanonical method with the well known simulated annealing for the effectiveness in search of the energy global minimum of a biomolecular system. For this we study in detail Met-enkephalin, one of the simplest peptides. We show that the new method not only outperforms simulated annealing in the search of the energy groundstate but also provides more statistical-mechanical information about the system.

1 INTRODUCTION

Systems with frustration are commonly present in many fields of science and engineering. To name a few, spinglass, neural network, protein folding, traveling salesperson problem, and optimal wiring of electric circuits are the examples of such systems. These systems belong to the same class of the so-called NP complete optimization problem where the number of computing steps required to solve the problem increases faster than any power of the size of the system. The problem is simply stated as follows: Find the global minimum out of a huge number of local minima separated by high tunneling barriers.

In this article, we compare two effective methods, simulated annealing [1] and multicanonical algorithms [2, 3], in the study of a system of frustration by taking the example of the protein folding problem. The prediction of the three-dimensional structure of proteins solely from their amino acid sequences remains one of the long-standing unsolved problems in biophysics (for a recent review, see, for example, Ref. [4]). Traditional methods such as molecular dynamics and Monte Carlo simulations at relevant temperatures tend to get trapped in local minima. A now almost classical way to alleviate this difficulty is simulated annealing.[1] Simulated annealing was proposed to be used to predict the global minimum-energy conformations of polypeptides and proteins [5]-[7] and refine protein structures from NMR and X-ray data.[8]-[10] Since then many promising results have been obtained.[11]-[26]

Recently the authors proposed another approach, the multicanonical method [2, 3], to the protein folding problem.[27] This new ansatz was successfully tested for systems with first-order phase transitions [3, 28, 29] and spin glasses [30]-[34] where one has to deal with similar multiple-minima problems. The core of this ansatz is to perform Monte Carlo simulations in a *multicanonical* ensemble [3] instead of the usual (canonical) Gibbs-ensemble. In the new ensemble the energy is forced on a one-dimensional random walk and so a simulation can overcome the energy barriers between local minima by connecting back to the high temperature states. The canonical distribution for *any* temperature can be obtained by the re-weighting techniques.[35] In a pilot study [27] the authors demonstrated for a small peptide that the new approach allows indeed both the identification of

groundstates and the calculation of thermodynamic quantities over a wide temperature range from just one simulation.

In this paper we like to compare the performance of the multicanonical ansatz with the older simulated annealing. For this test we chose the system of Met-enkephalin, one of the simplest peptides, since its lowest-energy conformation for the potential energy function ECEPP/2 [36]-[38] is known.[39] As another task we like to study the thermodynamic properties of this peptide in greater detail.

The paper is organized as follows. In Section 2 we briefly review simulated annealing and different variants of the multicanonical method. In Section 3 we give the computational details. In Section 4 we present our results for the exploration of groundstates and compare the different optimization methods. Later in the Section we try to evaluate physical quantities of the peptide over a large temperature range. Conclusions and discussion are given in Section 5.

2 ALGORITHMS

2.1 Simulated Annealing

Today, simulated annealing [1] is one of the most widely used methods in solving global optimization problems. The method is based on the "crystal forming" process; during a simulation temperature is lowered very slowly from a sufficiently high initial temperature T_0 where the structure changes freely with Monte Carlo updates to a "freezing" temperature T_f where the system undergoes no significant changes with respect to the Monte Carlo iteration. If the rate of temperature decrease is slow enough for the system to stay in thermodynamic equilibrium, then it is ensured that the system can avoid getting trapped in local minima and that the global minimum will be found. However, the simulation should be monitored closely and the annealing should be tailored very carefully to achieve this condition.[23] This causes a great increase in required computation time especially at low temperatures, and so it is often run with a simple annealing protocol without a careful testing of thermal equilibrium. Hence, the relationship of the obtained conformations to the the calculation of thermodynamic quantities will be hampered by uncontrolled bias. For this reason, a certain number (which is not known *a priori*) of

runs are necessary to evaluate the performance and to make sure that the obtained final conformations are close to the global minimum.

In the present simulation the temperature was lowered exponentially in $NSTEP$ times by setting the inverse temperature $\hat{\beta} = 1/k_B T$ to

$$\hat{\beta}_n = \hat{\beta}_0 \gamma^n \ , \tag{1}$$

for the nth temperature step ($n = 0, 1, ...$). Here, $\hat{\beta}_0$ is the initial inverse temperature and γ is given by

$$\gamma = \left(\frac{\hat{\beta}_f}{\hat{\beta}_0} \right)^{\frac{1}{NSTEP}} \ , \tag{2}$$

In the present work, for the purpose of comparison, we made a fixed number of Monte Carlo sweeps, N_T, at each temperature step so that the total number of Monte Carlo sweeps per run, $NSWEEP$, is fixed:

$$NSWEEP = N_T \times NSTEP \ . \tag{3}$$

For a fixed value of $NSWEEP$, these constants ($\hat{\beta}_0$, $\hat{\beta}_f$, and $NSTEP$) are free parameters and have to be tuned in such a way that the annealing process is optimized for the specific problem. In the present work, we set the initial temperature T_0 to be 1000 K and compared the cases for a few choices of $NSTEP$ and the final temperature T_f.

2.2 Multicanonical Ensemble

In the canonical ensemble, configurations at an inverse temperature $\hat{\beta} \equiv 1/k_B T$ are weighted with the Boltzmann factor $w_B(E) = \exp\left(-\hat{\beta}E\right)$. The resulting probability distribution is given by

$$P_B(E) \ \propto \ n(E) w_B(E) \ , \tag{4}$$

where $n(E)$ is the spectral density. In the *multicanonical* ensemble, [3] on the other hand, the probability distribution is *defined* by the condition

$$P_{mu}(E) \ \propto \ n(E) w_{mu}(E) = \text{const.} \tag{5}$$

Hence, all energies have equal weight and a one-dimensional random walk in energy space is realized (when simulated with local updates), which insures that the system can over-

come any energy barrier. Note that from Eq. (5) we have

$$w_{mu}(E) \propto n^{-1}(E) . \tag{6}$$

Unlike for the canonical ensemble the multicanonical weight factor $w_{mu}(E)$ is not *a priori* known, and one needs its estimator for a numerical simulation. Hence, the multicanonical ansatz consists of three steps: In the first step the estimator of the multicanonical weight factor is calculated. Then one performs with this weight factor a multicanonical simulation with high statistics. The standard Markov process (for instance, in a Metropolis update scheme [40]) is well-suited for generating configurations which are in equilibrium with respect to the multicanonical distribution. Finally, from this simulation one can not only locate the energy global minimum but also obtain the canonical distribution at any inverse temperature $\hat{\beta}$ for a wide range of temperatures by the re-weighting technique:[35]

$$P_B(\hat{\beta}, E) \propto w_{mu}^{-1} P_{mu}(E) e^{-\hat{\beta}E} . \tag{7}$$

The crucial point is the first step: calculating the estimator for the multicanonical weight factor $w_{mu}(E)$. This can be done by the following iterative procedure:[2, 27]

1. Perform a canonical Monte Carlo simulation at a sufficiently high temperature T_0. In our case we chose $T_0 = 1000$ K. The weight factor for this simulation is given by $w(E) = e^{-\hat{\beta}_0 E}$ with $\hat{\beta}_0 = 1/k_B T_0$. Initialize the array $S(E)$ to zero, where E is discretized with bin width δE (= 1 kcal/mol in the present work).

2. Sample the energy distribution obtained in the previous simulation as a histogram $H(E)$ with the same bin width as in $S(E)$. In the first iteration (step 1 above) determine E_{max} as the value near the mode where the histogram has its maximum. (E_{max} is fixed throughout the iterations.) Let E_{min} be the lowest energy ever obtained. For all $H(E)$ with entries greater than a minimum value (say, 20) and $E_{min} \leq E \leq E_{max}$, update the array $S(E)$ by

$$S(E) = S(E) + \ln H(E) . \tag{8}$$

Note that $S(E)$ is for $\hat{\beta}_0 = 0$ an estimator of the microcanonical entropy.

3. Calculate the following multicanonical parameters $\alpha(E)$ and $\beta(E)$ from the array $S(E)$:

$$\beta(E) = \begin{cases} \hat{\beta}_0 & , \ E \geq E_{max} \\ \hat{\beta}_0 + \dfrac{S(E') - S(E)}{E' - E} & , \ E_{min} \leq E < E' < E_{max} \\ \beta(E_{min}) & , \ E < E_{min} \end{cases} \tag{9}$$

and

$$\alpha(E) = \begin{cases} 0 & , \ E \geq E_{max} \\ \alpha(E') + (\beta(E') - \beta(E))E' & , \ E < E_{max} \end{cases} \tag{10}$$

where E and E' are adjacent bins in the array $S(E)$.

4. Start a new simulation with the multicanonical weight factor defined by

$$w_{mu}(E) = e^{-\beta(E)E - \alpha(E)} \ . \tag{11}$$

5. Iterate the last three steps until the obtained distribution $H(E)$ becomes reasonably flat in the chosen energy range. Inserting Eq. 9 and Eq. 10 in Eq. 11 one can easily show that the multicanonical weight factor $w_{mu}(E)$ will become proportional to the inverse spectral density in the choosen energy range as it is required by its definition (see Eq. 6).

While this method for determining the multicanonical weight factor $w_{mu}(E)$ is quite general, it has the disadvantage that it requires a certain number of iterations which is not *a priori* known. For the calculations in Ref. [27] about 40 % of the total CPU time was spent for this part. We remark that the above method of calculating multicanonical weights is by no means unique. Especially it is not necessary to choose the parametrization of Eq. (11) for the multicanonical weight factor. However, with this parametrization and its introduction of "effective" temperatures $\beta(E)$ the connection to the canonical ensemble becomes very clear.

2.3 Multicanonical Annealing

If one is just interested in the groundstate structure it may be worthwhile to use instead a variant of the multicanonical method, *multicanonical annealing.* [41] Multicanonical annealing alleviates the above-mentioned complication of determination of the multicanonical weight factor. However, because of this simplification, it does not allow any

calculation of thermodynamic quantities. It was first proposed for the traveling salesperson problem, one of the classical examples of an NP-complete optimization problem. First applications to the protein folding problem exists, too.[42] Results better than those obtained by simulated annealing were reported.

In simulated annealing, directed moves are achieved by gradually lowering the temperature. For multicanonical annealing, we introduce an upper bound in energy at the other end of the annealing direction, rejecting all attemps beyond this bound. Annealing is achieved by moving the bound in the annealing direction while keeping the sampling interval ΔE fixed. Within this energy interval the system can move out of local minima as long as their barrier heights do not exceed the upper limit of the energy range. The algorithm can be implemented in the following way: [41, 42]

1. Perform a short canonical Monte Carlo (MC) simulation at a sufficiently high temperature T_0. Again we chose $T_0 = 1000$ K in the present work. Initialize an array $S(E)$ to zero, where E is discretized with bin width δE (= 1 kcal/mol in the present work).

2. Sample the energy distribution obtained in the previous simulation as a histogram $H(E)$. Let E_{min} be the lowest energy ever obtained. Calculate

$$S(E) = S(E) + \ln H(E) \ . \tag{12}$$

3. Update the upper bound E_{wall} of the sampling interval by

$$E_{wall} = \max(E_{last}, E_{min} + \Delta E) \tag{13}$$

where ΔE is the size of the sampling energy range and E_{last} the energy of the last configuration.

4. Calculate the following parameter β_{min} by:

$$\beta_{min} = \frac{S(E_{wall}) - S(E_{min})}{E_{wall} - E_{min}} \tag{14}$$

5. Define the new weight factor by

$$w(E) = \begin{cases} 0 & , \ E > E_{wall} \\ e^{-S(E)} & , \ E_{min} \leq E \leq E_{wall} \\ e^{-S(E_{min}) - \beta_{min}(E - E_{min})} & , \ E < E_{min} \end{cases} \tag{15}$$

and start a new simulation with this weight factor with the last configuration of the preceding simulation as the initial structure.

6. Iterate the last four steps till some convergence criterion is met.

In the present work, for the purpose of comparison with other methods, we set the number of annealing iterations to a fixed value (instead of checking the convergence criterion). If we call this number $NSTEP$ and the number of MC sweeps per iteration N_T, then the number of MC sweeps per run, $NSWEEP$, is given by Eq. (3).

Because of the finite interval size ΔE, the MC procedure will no longer be ergodic and it is not possible to find the equilibrium properties of the system. Hence, the canonical distribution cannot be reconstructed. For the purpose of annealing this does not matter as long as one chooses the sampling interval large enough to allow important fluctuations throughout the annealing process. However, since ergodicity is not fulfilled, one has to repeat the annealing process many times with different initial configurations, to make sure that one has found a good approximation to the global minimum. Conventional simulated annealing has to cope with the same problem. As in simulated annealing, where one does not know *a priori* the optimal cooling schedule, the optimal sampling interval size ΔE is not known *a priori* for multicanonical annealing and has to be chosen on a trial and error basis. The problem can be eased by making the sampling interval size itself a dynamical variable which is changed according to the following rule in the annealing process. We preset the sampling interval size ΔE to a given minimum value Δ_m and double it every time when the simulation does not find a new global-minimum candidate for three consecutive steps. Once a better estimate of the global minimum is found, ΔE is reset to its initial value Δ_m.

In the present work, we try to compare the performances of the above three methods, simulated annealing, regular multicanonical algorithm, and multicanonical annealing.

3 COMPUTATIONAL DETAILS

3.1 Potential Energy Function

Met-enkephalin has the amino-acid sequence Tyr-Gly-Gly-Phe-Met. For our simulations the backbone was terminated by a neutral NH_2- group at the N-terminus and a neutral $-COOH$ group at the C-terminus as in the previous works of Met-enkephalin.[6, 17, 20, 27, 39] The potential energy function E_{tot} that we used is given by the sum of the electrostatic term E_{es}, 12-6 Lennard-Jones term E_{vdW}, and hydrogen-bond term E_{hb} for all pairs of atoms in the peptide together with the torsion term E_{tors} for all torsion angles.

$$E_{tot} = E_{es} + E_{vdW} + E_{hb} + E_{tors}, \tag{16}$$

$$E_{es} = \sum_{(i,j)} \frac{332 q_i q_j}{\epsilon r_{ij}}, \tag{17}$$

$$E_{vdW} = \sum_{(i,j)} \left(\frac{A_{ij}}{r_{ij}^{12}} - \frac{B_{ij}}{r_{ij}^{6}} \right), \tag{18}$$

$$E_{hb} = \sum_{(i,j)} \left(\frac{C_{ij}}{r_{ij}^{12}} - \frac{D_{ij}}{r_{ij}^{10}} \right), \tag{19}$$

$$E_{tors} = \sum_{l} U_l \left(1 \pm \cos(n_l \alpha_l)\right), \tag{20}$$

where r_{ij} is the distance between the atoms i and j, and α_l is the torsion angle for the chemical bond l. The parameters ($q_i, A_{ij}, B_{ij}, C_{ij}, D_{ij}, U_l$ and n_l) for the energy function were adopted from ECEPP/2.[36]-[38] The effect of surrounding atoms of water was neglected and the dielectric constant ϵ was set equal to 2. The computer code KONF90 [14, 15] was used. The peptide-bond dihedral angles ω were fixed at the value 180° for simplicity, which leaves 19 angles ϕ_i, ψ_i, and χ_i as independent variables. Because of this choice and a different convention for the implementation of the ECEPP parameters (for example, ϕ_1 of ECEPP/2 is equal to $\phi_1 - 180°$ of KONF90, and energies are also different by small irrelevant constant terms), our results slightly differ from the one in Ref. [39] which were obtained by another method but can be directly compared with Refs. [20] and [27].

3.2 Implementation of the Algorithms

Preliminary runs showed that all methods need roughly the same amount of CPU time for a fixed number of MC sweeps (about 15 minutes for 10,000 sweeps on an IBM RS6000 320H). Hence, we compared the different methods by performing simulations with the same number of total MC sweeps. By setting this number to 1,000,000 sweeps we tried to ensure high statistics. Note that the statistics for each method are therefore 2.5 times more than those of Ref. [20]. One MC sweep updates every dihedral angle of the peptide once.

For simulated annealing and multicanonical annealing, one problem is to find the optimal annealing schedules. For each choice of the annealing parameters, (the final temperature and number of temperature steps for simulated annealing and the sampling interval size and number of annealing iterations for multicanonical annealing), we performed 10 simulations with $NSWEEP = 100,000$ (so that the total number of MC sweeps is equal to 1,000,000). Each simulation started with a different random initial conformation. For certain cases, we also performed 20 runs with $NSWEEP = 50,000$ in order to see the dependence of the methods on $NSWEEP$.

For simulated annealing the initial temperature was $T_0 = 1000$ K and the temperature was exponentially decreased according to Eq. (1). We compared the cases for three values of $NSTEP$ ($NSTEP = NSWEEP$, 50, and 20) and two final temperatures ($T_f = 50$ and 1 K). The case for $NSTEP = NSWEEP$ is the protocol of Ref. [15], and it represents the slowest and smoothest annealing schedule (the factor γ in Eq. (1) is equal to $1.000029\cdots$ for $T_f = 50$ K and $NSWEEP = 100,000$). The cases for $NSTEP = 50$ ($\gamma = 1.0630\cdots$ for $T_f = 50$ K) and for $NSTEP = 20$ ($\gamma = 1.1707\cdots$ for $T_f = 50$ K) are essentially the protocol of Ref. [13].

For multicanonical annealing we divided the 100,000 MC sweeps of each run in 10 annealing iterations of 10,000 sweeps for the case of fixed sampling interval and in 20 steps of 5,000 sweeps for the case of dynamically changed sampling size. For the former case, we compared three values of the sampling interval size ΔE ($\Delta E = 5$, 10, and 15 kcal/mol), and for the latter case, we compared two values of the minimal sampling size Δ_m ($\Delta_m = 5$ and 10 kcal/mol).

For regular multicanonical simulation we used the same weight factor as that already determined by four iterative steps of 10,000 sweeps each in Ref. [27]. All thermodynamic quantities were then calculated from a production run of 9,960,000 sweeps which includes 10,000 sweeps for thermalization. At the end of every second sweep we stored the actual configuration and the energy for future analysis of thermodynamic quantities. Note that the fraction of CPU time needed for calculating the multicanonical weight factor can now be restated to be only 4 % (instead of 40 % in Ref. [27]).

4 RESULTS

4.1 Groundstate Investigations

First, we have to define the groundstate of enkephalin. In Ref. [20] it was shown that with KONF90, conformations with energies less than -11.0 kcal/mol have essentially the same structure (Type A of Ref. [20]). Hence, we consider any conformation with $E < -11.0$ kcal/mol as the groundstate configuration.

In our production run for regular multicanonical simulations we observed 18 tunneling events where a tunneling event means that the system went from the groundstate region (energies less than -11.0 kcal/mol) to E_{max} (above which the multicanonical parameters are set to $\alpha(E) = 0$ and $\beta(E) = \hat{\beta}_0 = 1/k_B T_0$ with $T_0 = 1000$ K) and came back to the groundstate region. Here, we set $E_{max} = 20$ kcal/mol. When the system reaches E_{max} region, it has to stay a certain amount of time with which the simulation is updated according to the Boltzmann weight for a very high temperature ($T_0 = 1000$ K). Hence, the system will encounter enough randomness to ensure that groundstate configurations separated by such a tunneling event are statistically independent. For this reason, the number of tunneling events gives a lower bound for the number of independent groundstate configurations found by this method. Table 1 summarizes our results. For each tunneling event the estimated groundstate energy E_{GS} was chosen to be the lowest energy obtained in the corresponding cycle. The 18 estimated groundstate structures were all essentially the same, by which we mean their dihedral angles (ϕ_i, ψ_i, and χ_i) differ less than ≈ 10 degrees. From the table we found as a tunneling time $\tau_{tu} = 54136 \pm 8187$, measured in MC sweeps. This value is high for such a small peptide as Met-enkephalin. This is caused

by the high rejection rate and small energy changes of the accepted Metropolis steps at low energy regions. But one has to remember that the use of the multicanonical ensemble is not restricted to local Metropolis updates. Work is under progress to accelerate the method by using collective updates.

In Table 2 we list the results obtained by simulated annealing for the lowest energies, the number of times a groundstate configuration (with energy $E \leq -11.0$ kcal/mol) was found, and the average of their lowest energy estimates. The results are from 10 runs with $NSWEEP = 100,000$ per run. The annealing schedules were tested for three different choices of $NSTEP$ (= $NSWEEP$, 50, and 20) and two different choices of the final temperature T_f (= 50 K and 1 K), where $NSTEP$ is the number of different temperatures considered in the annealing process (see Eqns. (1)-(3)). The first thing one can read off from the table is that the results are similar from one annealing schedule to another (no order-of-magnitude differences). However, the results imply the following qualitative tendencies. First of all, when the annealing is fast ($NSTEP = 20$), the probability of finding the global minimum decreases compared to the case for slower annealing ($NSTEP = NSWEEP$ and 50). Secondly, if the final temperature is too low, then the cooling will also be fast and with a certain probability simulated annealing will get trapped in some metastable states. We observed this for the final temperature $T_f = 1$ K where we found either no improvement or even worse results than those for $T_f = 50$ K. On the other hand, if the final temperature is too high, then the probability of finding the global minimum is also low. For the final temperature $T_f = 300$ K simulated annealing failed in finding a groundstate (data not shown). Hence, the optimal final temperature for the present case is around 50 K.

In Table 3 we list the same quantities obtained by simulated annealing for less number of sweeps per run ($NSWEEP = 50,000$) with the continuous annealing ($NSTEP = NSWEEP$). The results are worse for $T_f = 50$ K compared to those in Table 2 (the probability of finding the groundstate decreasing from 50 % to 30 % by the reduction of the number of sweeps per run). The situation is clearer if we compare these results with those from 100 runs of 10,000 sweeps each (data not shown). In the latter case, we found groundstates only 13 times (13 %), and the average of the lowest energy was

$< E >= -8.4(1.7)$ kcal/mol. Hence, the optimal choice for $NSWEEP$ is definitely more than 10,000 and probably more than 100,000.

We now discuss the results for multicanonical annealing. In Table 4 we list the lowest energies, the number of times a groundstate configuration was found, and the average of their lowest energy estimates. The results are from 10 runs with $NSWEEP = 100,000$ per run. They strongly depend on the choice of the parameters that rule the annealing procedure. In particular, one has to choose the sampling energy interval ΔE large enough. The probability to find the groundstate increases with ΔE from 30 % for $\Delta E = 5$ kcal/mol to 100 % for $\Delta E = 15$ kcal/mol. The probability also increases from 80 % for minimal sampling energy interval $\Delta_m = 5$ kcal/mol to 100 % for $\Delta_m = 10$ kcal/mol for the case of dynamically changed sampling size.

In Table 5 we list the same quantities obtained by multicanonical annealing with less number of sweeps per run ($NSWEEP = 50,000$) for the optimal choices of sampling sizes from Table 4. We performed 10 annealing steps of 5,000 sweeps each for the case of fixed sampling interval size and 20 annealing steps of 2,500 sweeps for the case of dynamically changed sampling size. As noted for the case of simulated annealing, the results are worse by reducing the number of sweeps per run; the probability of finding the groundstate decreases probably between 50,000 and 100,000.

We now compare the results for simulated annealing and multicanonical annealing (Tables 2–5). First, we observe that the probability of finding the groundstate was 100 % for the optimal cases of multicanonical annealing, while that for simulated annealing was 50 %. Secondly, the average $< E >$ is generally smaller and fluctuates less for multicanonical annealing than for simulated annealing. This is true even in the cases where both methods found the same number of groundstate configurations (compare the results for $\Delta E = 10$ kcal/mol in Table 4 and those for $T_f = 50$ K in Table 2). Hence, we conclude that the multicanonical annealing is superior to simulated annealing. However, the improvement is not as impressive as it was quoted for the traveling salesperson problem in Ref. [41]. The superiority of multicanonical annealing to simulated annealing can be understood by the fact that the sampling interval for multicanonical annealing is essentially constant, while it shrinks with decreasing temperature for simulated annealing.

Hence, the chance of escaping from a local minimum is much larger for multicanonical annealing.

On the other hand, there seem to be no significant advantage of multicanonical annealing over a regular multicanonical algorithm. The maximum numbers of independent groundstate configurations found by a regular multicanonical simulation ($n_{GS} = 19$) and multicanonical annealing ($n_{GS} = 18$) are almost the same (see Tables 1 and 5). Since a regular multicanonical simulation provides additional information about the thermodynamics of the system, it seems that this method is the best choice. The situation may be different for spin glasses and the traveling salesperson problem where one always has to study different realizations of the systems. Namely, one has to recalculate the multicanonical weight factor for each realization anew and therefore it can be computationally easier to use multicanonical annealing.

To conclude this section, we discuss another application of multicanonical annealing: its use for the determination of the heights of barriers between different local minima. In Ref. [20] it was observed that there is another characteristic local minimum around energy -10.0 kcal/mol (type B in Ref. [20]) whose structure is significantly different from the groundstate structure (type A in Ref. [20]). We took one of this type B conformations as the initial conformation and made a set of multicanonical annealing runs with 100,000 Monte Carlo sweeps for various values of the sampling interval size ΔE. The results are presented in Table 6. They imply that the sampling interval size has to be more than 14 kcal/mol, before the system is able to find the groundstate. Hence, the barrier height which separates the configurations of type A and type B is between -14 and -15 kcal/mol. Note that we can see this clearly in the results for fixed sampling interval size in Table 4. For $\Delta E = 5$ and 10 kcal/mol the simulation cannot get out of a local minimum once it falls in it, but for $\Delta E = 15$ kcal/mol simulation can overcome the energy barriers and always find the groundstate ($n_{GS} = 10$). This kind of analysis should allow one to study in more detail the relation between the groundstate and long-living metastable state with only slightly higher energy.

4.2 Calculating Thermodynamic Quantities

In the previous subsection, we concentrated solely on the ability of the different algorithms to explore the groundstate of the peptide. In this section we like to demonstrate in more detail how the regular multicanonical method (not multicanonical annealing) is able to estimate thermodynamic quantities over a wide range of temperatures. This amazing new feature results from the fact that it is possible to reconstruct the canonical distribution at various temperatures from one multicanonical simulation (see Eq. (7)). As an example we show in Fig. 1 the probability distribution as a function of the temperature that was obtained by the multicanonical production run with 1,000,000 MC sweeps. As expected, there is a conspicuous peak in probability around $E = -11$ kcal/mol near $T = 0$ K. In principle, one could also reconstruct the canonical distribution from simulated annealing runs provided that the annealing schedule is monitored very carefully.[23] However, in practice this constraint is difficult to realize and introduces hard-to-control systematic errors in the calculation of thermodynamic quantities. As an example we show in Fig. 2a and Fig. 2b the probability distribution at $T = 300$ K and $T = 50$ K as obtained by a canonical simulation, a multicanonical simulation, and simulated annealing. All simulations relied on 1,000,000 sweeps. In the cases of canonical simulation and simulated annealing, our results are from 20 runs of 50,000 sweeps with different random start-configurations. Only the final conformations were taken into account for these cases, and so the results are very crude estimate of the probability distribution. For the multicanonical case, on the other hand, not only the final conformation but also all other intermediate conformations were taken into account through reweighting. For 300 K the multicanonical simulation reproduced the distribution as obtained directly by a canonical distribution while simulated annealing gives a much rougher approximation. For 50 K the canonical simulation got trapped in a local minimum and did not reach the equilibrium and is far away from the distribution as predicted by the multicanonical simulation which is not affected by this problem. But simulated annealing also failed in reproducing this distribution. The center of the two distributions (obtained by multicanonical simulation and simulated annealing) differ by ≈ 2 kcal/mol. This demonstrates clearly that calculating thermodynamic quantities from simulated annealing runs is dangerous and requires a careful monitoring of

the annealing to provide reliable results. On the other hand, multicanonical simulations are not hindered by this problem and we can use them to calculate a variety of physical quantities.

An important quantity one likes to monitor as a function of temperature is the average energy of the peptide. This energy is a sum of four terms: Coulomb-energy E_{es}, hydrogen-bond energy E_{hb}, van der Waals energy E_{vdW} and torsion energy E_{tor} (see Eqns. (16)–(20)). In Fig. 3 we display expectation values of these terms and the total energy E_{tot} as a function of the temperature. One clearly observes that the behavior of the energy E_{tot} is dominated by the van der Waals term. [25] While the behavior of the energy is smooth and slowly changing, we observe a pronounced peak in the specific heat, defined by

$$C(\hat{\beta}) = \hat{\beta}^2 \frac{< E^2 > - < E >^2}{5} \tag{21}$$

(see Fig. 4), a phenomenon common to phase transitions in statistical physics. An important question is if the peak is indeed a signal for a phase transition. Of course our peptide is a finite system and much too small to speak of a phase transition in the sense the word is used in statistical physics, but one can imagine that the peak indicates a crossover between a "folded" and a disordered structure which could for larger proteins be interpreted as a phase transition.

To study this question one first has to find a quantity which can serve as an order parameter. A natural definition of such an order parameter is inspired by the Parisi order parameter for spin glasses: the overlap of two configurations separated by an infinitely long time:

$$Op = \frac{1}{N_\alpha} \sum_\alpha \cos(\alpha(t) - \alpha(t + \infty)), \tag{22}$$

where the sum goes over all N_α dihedral angles $\alpha \in (\phi, \psi, \chi)$ (here, $N_\alpha = 19$). This definition is by no means unique. For instance one could also choose

$$Op = \frac{1}{N_\alpha} \sum_\alpha \delta(\alpha(t), \alpha(t + \infty)), \tag{23}$$

where $\delta(\alpha_i, \alpha_j) = 1$, if $|\alpha_i - \alpha_j| < D$ and 0 in all other cases, with D a certain upper bound (say, 20 degrees). Another way to calculate our "order parameter" would be to perform two simulations of the same system with different start configurations (replicas

in the language of spin glasses):

$$Op = \frac{1}{N_\alpha} \sum_\alpha \cos(\alpha^{(1)} - \alpha^{(2)}), \tag{24}$$

where the superscript marks the different replicas. Since both replicas are totally uncorrelated they can be regarded as the same system separated by an infinitely long time. We remark that similar order parameters for the system of a biomolecule were considered by other workers, too. [43, 23]

In the present work, we take the definition of Eq. (23) for the order parameter. We approximated the requirement of infinitely long separation of the configurations by taking the overlap of the first 100,000 sweeps after thermalization with the last 100,000, so that both sets are separated by 750,000 sweeps. This is much more than necessary, since every tunneling event marks a new set of statistically independent configurations, and we had 19 tunneling events altogether (see Table 1). Fig. 5 displays the average of the order parameter as a function of the temperature T. It seems that our "order parameter" allows to describe in a general way the crossover between the folded state and the coil state. The step-like behavior of this quantity should become even steeper for a system with a phase transition. However, unlike for spinglasses one always finds only one state and not a multitude of different groundstates for low temperatures. This can be seen in Fig. 6 where we display the order parameter distribution as a function of temperature. Note that even for high temperatures the mean of the distribution is not at zero as for spin systems. This is due to the fact that geometric constraints make certain angular values highly unfavorable.

In order to further elucidate the behavior of the order parameter we now define a configuration as groundstate-like if 14 (or 74 %) of the dihedral angles differ by less than 20 degrees from the lowest-energy configuration ever encountered (type A in Ref. [20]). We likewise define a coil configuration as one where less than 5 of the dihedral angles fullfil the above condition. All other configurations are considered as intermediate. Fig. 7 displays the percentage of the different types of configurations as a function of temperature. The percentage of groundstate configurations is maximal for low temperatures and decreases fast around room temperatures. On other hand, the high temperature region

is dominated by coil structures, while the intermediate structures occur mostly at temperatures around 300 K. We also studied how often the configurations of types B and C of Ref. [20] appear, but found that these configurations have no significant contributions. Only for temperatures around 250 K we found, that about 2 % of the configurations were of type B, otherwise their number was always negligible. To study in more detail the mechanism of the crossover between the ordered structure and the random structure we investigate the free energy differences ΔG, enthalpy differences ΔH and entropy differences ΔS between groundstate-like configurations and coil structures. The enthalpy difference was estimated by the difference in potential energy. First, we display in Fig. 8 the enthalpy differences ΔH. We find that the enthalpy differences between intermediate configurations and coil configurations are much smaller than those between groundstate configurations and intermediate configurations or between groundstate configurations and coil structures. Over the whole energy range the groundstate is energetically favored, but this is different for the free energy or entropy. The free energy differences were calculated from

$$\Delta G = -\beta^{-1} \ln \frac{N_A}{N_B}, \tag{25}$$

where N_A and N_B are the average numbers of configurations in states A and B, respectively. Finally, the entropy differences were obtained from

$$T\Delta S = \Delta H - \Delta G \ . \tag{26}$$

As one can see from Fig. 9 coil structures are favored by entropy. Again the differences between intermediate configurations and coil structures are much smaller than between groundstates and coils or between groundstates and intermediate structures. For temperatures below room temperature the entropy difference between intermediate configurations and coil configurations vanishes. For temperatures below 150 K the entropy difference between groundstates and coil configuration is also compatible with zero. Since intermediate states and coil structures have similar entropy and energy we treat them now as the same type of configurations and compare the groundstate configurations with non-groundstate configurations. In Fig. 10 we display the enthalpy, and entropy differences between both types of configurations. Again one can see that the thermodynamic

behavior of the peptide is dominated for high temperatures by the entropy, favoring non-groundstate-like structures. Hence, we observe large positive free energy differences ΔG. On the other hand at low temperatures energy dominates and favors groundstate-like structures, yielding negative free energy differences ΔG. Around room temperature ΔG is small, groundstate-like configurations and others appear with similar probability. This explains the large fluctuations in the total energy visible in the peak in the specific heat.

5 CONCLUSIONS AND DISCUSSION

By performing a simulation with Met-enkephalin, we studied the performances of a few variants of the multicanonical approach and compared them with simulated annealing. It was shown that the multicanonical method allows a more efficient search for the ground-state. Even more important, multicanonical simulation allows one to study the thermodynamic behavior of biological molecules over a wide range of temperatures from just one simulation, which was not possible by other methods. We demonstrated this by calculating various physical quantities as a function of temperature and estimated differences in the free energy, enthalpy, and entropy between groundstate-like configurations and other configurations.

Acknowledgements:

Our simulations were performed on clusters of fast RISC workstations at SCRI (The Florida State University, Tallahassee, USA) and HITAC S820/80 at National Institute for Molecular Science, Okazaki, Japan. This work is supported, in part, by the Department of Energy, contract DE-FC05-85ER2500, by a Grant-in-Aid for Scientific Research from the Japanese Ministry for Education, Science and Culture, by the Konrad-Zuse-Zentrum für Informationstechnik Berlin (ZIB) and by MK Industries, Inc. Part of this work was written while one of us (U. H.) was summer visitor at Brookhaven National Laboratory. U. H. likes to thank BNL for the kind hospitality extended to him.

References

[1] S. Kirkpatrick, C.D. Gelatt, Jr., and M.P. Vecchi, *Science*, **220**, 671 (1983).

[2] B.A. Berg and T. Neuhaus, *Phys. Lett.*, **B267**, 249 (1991).

[3] B.A. Berg and T. Neuhaus, *Phys. Rev. Lett.*, **68**, 9 (1992)

[4] M. Levitt, *Curr. Opin. Struct. Biol.*, **1**, 224 (1991).

[5] S.R. Wilson, W. Cui, J.W. Moskowitz, and K.E. Schmidt, *Tetrahedron Lett.*, **29**, 4373 (1988).

[6] H. Kawai, T. Kikuchi, and Y. Okamoto, *Protein Eng.*, **3**, 85 (1989).

[7] C. Wilson and S. Doniach, *Proteins*, **6**, 193 (1989).

[8] M. Nilges, G.M. Clore, and A.M. Gronenborn, *FEBS Lett.*, **229**, 317 (1988).

[9] A.T. Brünger, *J. Mol. Biol.*, **203**, 803 (1988).

[10] A.T. Brünger, M. Karplus, and G.A. Petsko, *Acta Cryst.*, A**45**, 50 (1989).

[11] P. Affinger and G. Wipff, *J. Comp. Chem.*, **11**, 19 (1990).

[12] D.S. Goodsell and A.J. Olson, *Proteins*, **8**, 195 (1990).

[13] S.R. Wilson and W. Cui, *Biopolymers*, **29**, 225 (1990).

[14] H. Kawai, Y. Okamoto, M. Fukugita, T. Nakazawa, and T. Kikuchi, *Chem. Lett.*, **1991**, 213.

[15] Y. Okamoto, M. Fukugita, T. Nakazawa, and H. Kawai, *Protein Eng.*, **4**, 639 (1991).

[16] M. Fukugita, T. Nakazawa, H. Kawai, and Y. Okamoto, *Chem. Lett.*, **1991**, 1279.

[17] B. von Freyberg and W. Braun, *J. Comp. Chem.*, **12**, 1065 (1991).

[18] K.-C. Chou and L. Carlacci, *Protein Eng.*, **4**, 661 (1991)

[19] T. Nakazawa, H. Kawai, Y. Okamoto, and M. Fukugita, *Protein Eng.*, **5**, 495 (1992).

[20] Y. Okamoto, T. Kikuchi, and H. Kawai, *Chem. Lett.*, **1992**, 1275.

[21] D.G. Garrett, K. Kastella, and D.M. Ferguson, *J. Am. Chem. Soc.*, **114**, 6555 (1992).

[22] T. Nakai, A. Kidera, and H. Nakamura, *J. Bio. NMR*, **3**, 19 (1993).

[23] D.G. Garrett, K. Kastella, and D.M. Ferguson, *Analyzing the Physical Properties of Simplified Protein Models: A Novel Application of Simulated Annealing-Optimal Histogram Methods and Spin Glass-Overlap Functions*, Minnesota Supercomputer Institute Research Report UMSI 93/212.

[24] Y. Okamoto, T. Kikuchi, T. Nakazawa, and H. Kawai, *Int. J. Peptide Protein Res.*, **42**, 300 (1993).

[25] Y. Okamoto, *Proteins*, **19**, 14 (1994).

[26] Y. Okamoto, *Biopolymers*, **34**, 529 (1994).

[27] U.H.E. Hansmann and Y. Okamoto, *J. Comp. Chem.*, **14**, 1333 (1993).

[28] B. Berg, U. Hansmann and T. Neuhaus, *Phys. Rev.* **B 47**, 497 (1993).

[29] B. Berg, U. Hansmann and T. Neuhaus, *Z. Phys.* **B 90**, 229 (1993).

[30] B. Berg and T. Celik, *Phys. Rev. Lett.*, **69** 2292 (1992).

[31] B. Berg, T. Celik and U. Hansmann, *Europhysics Letters*, **22**, 63 (1993).

[32] B. Berg, T. Celik and U. Hansmann, *Groundstate Properties of the 3d Ising Spin Glass*, *Physical Review* **B**, in press.

[33] T. Celik, U.H.E. Hansmann and M. Katoot, *J. Stat. Phys.*, **73**, 775 (1993).

[34] U.H.E. Hansmann, T. Celik and M.Katoot, *Turk. J. Phys.*, **18**, 149 (1994).

[35] A.M. Ferrenberg and R.H. Swendsen, *Phys. Rev. Lett.*, **61**, 2635 (1988); **63** , 1658(E) (1989), and references given in the erratum.

[36] F.A. Momany, R.F. McGuire, A.W. Burgess, and H.A. Scheraga, *J. Phys. Chem.*, **79**, 2361 (1975).

[37] G. Némethy, M.S. Pottle, and H.A. Scheraga, *J. Phys. Chem.*, **87**, 1883 (1983).

[38] M.J. Sipple, G. Némethy, and H.A. Scheraga, *J. Phys. Chem.*, **88**, 6231 (1984).

[39] Z. Li and H.A. Scheraga, *Proc. Natl. Aca. Sci., U.S.A.*, **84**, 6611 (1987).

[40] N. Metropolis, A.W. Rosenbluth, M.N. Rosenbluth, A.H. Teller, and E. Teller, *J. Chem. Phys.*, **21**, 1087 (1953).

[41] J. Lee and M.Y. Choi, *Optimization by Multicanonical Annealing and the Traveling Salesman Problem*, preprint FSU-SCRI-93-107.

[42] U.H.E. Hansmann and Y. Okamoto, *Sampling Groundstate Configurations of a Peptide by Multicanonical Annealing*, preprint FSU-SCRI-94-30 and NWU-2/94, submitted for publication.

[43] E.I. Shakhnovich and A.M. Gutin, *Biophys. Chem.*, **34**, 187 (1989).

Table Captions:

Table 1: Estimated groundstate energies E_{GS} (in kcal/mol) of each tunneling event as obtained by a regular multicanonical simulation. t_{min} is the sweep when the simulation first entered the groundstate region ($E \leq -11.0$ kcal/mol) in the corresponding tunneling event. $< E >$ is the average of these estimates E_{GS}.

Table 2: Lowest energy (in kcal/mol) obtained by simulated annealing for three different choices of $NSTEP$ and two different choices of the final temperature T_f, where $NSTEP$ is the number of different temperatures considered in the annealing process (see Eqns. (1)–(3)). For all cases, the total number of Monte Carlo steps per run, $NSWEEP$, was 100,000. $< E >$ is the average of the lowest energy estimates and n_{GS} the number of runs in which a conformation with $E \leq -11.0$ kcal/mol was obtained.

Table 3: Lowest energy (in kcal/mol) obtained by simulated annealing with $NSTEP = NSWEEP$, where $NSTEP$ is the number of different temperatures considered in the annealing process and $NSWEEP$ is the total number of Monte Carlo steps per run. Here, we have $NSWEEP = 50,000$. Two different choices of the final temperature T_f (= 50 K and 1 K) were considered. $< E >$ is the average of the lowest energy estimates and n_{GS} the number of runs in which a conformation with $E \leq -11.0$ kcal/mol was obtained.

Table 4: Lowest energy (in kcal/mol) obtained by multicanonical annealing for different choices of the annealing sampling size ΔE. Δ_m is the minimal sampling size in the case where ΔE was changed dynamically. For all cases, the total number of Monte Carlo steps per run, $NSWEEP$, was 100,000. $< E >$ is the average of the lowest energy estimates and n_{GS} the number of runs in which a conformation with $E \leq -11.0$ kcal/mol was obtained.

Table 5: Lowest energy (in kcal/mol) obtained by multicanonical annealing for the best choices of the annealing sampling size ΔE and Δ_m in Table 4, where Δ_m is the minimal sampling size in the case where ΔE was changed dynamically. For all cases, the total number of Monte Carlo steps per run, $NSWEEP$, was 50,000. $< E >$ is the average of the lowest energy estimates and n_{GS} the number of runs in which a conformation with $E \leq -11.0$ kcal/mol was obtained.

Table 6: Type of lowest-energy structure and its energy E_m (in kcal/mol) obtained by

multicanonical annealing runs with various sampling interval size ΔE. The initial conformation for each run was that of a local minimum state (type B structure defined in Ref. [20]). Type A is a groundstate structure and has $E \leq -11.0$ kcal/mol.

Table 1.

n_{tu}	t_{min}	E_{GS}
0	22104	-12.0
1	78808	-11.9
2	123478	-12.0
3	211464	-12.0
4	267742	-12.1
5	299228	-12.1
6	372020	-11.6
7	375092	-12.1
8	445356	-12.1
9	499032	-12.0
10	553208	-11.9
11	569618	-11.4
12	655420	-12.0
13	673768	-12.0
14	781366	-11.3
15	796264	-11.9
16	875756	-12.0
17	971704	-11.8
18	977694	-12.1
$< E >$	—	$-11.9(2)$

Table 2.

	$NSTEP = 100,000$		$NSTEP = 50$		$NSTEP = 20$	
Run	$T_f = 50$ K	$T_f = 1$ K	$T_f = 50$ K	$T_f = 1$ K	$T_f = 50$ K	$T_f = 1$ K
1	−11.9	−8.0	−12.0	−11.2	−11.9	−10.9
2	−11.6	−11.9	−11.9	−9.1	−7.5	−11.8
3	−9.2	−8.5	−10.0	−8.3	−10.8	−9.0
4	−7.8	−8.0	−8.2	−10.0	−10.6	−12.2
5	−7.3	−12.2	−9.5	−12.2	−8.2	−7.9
6	−12.0	−9.8	−12.0	−11.2	−10.9	−10.0
7	−10.9	−10.3	−11.8	−10.6	−11.9	−9.1
8	−12.0	−11.1	−11.0	−12.2	−9.4	−7.1
9	−12.0	−10.3	−9.3	−8.6	−11.9	−8.5
10	−9.0	−8.6	−8.2	−12.2	−10.3	−9.0
$< E >$	−10.4(1.9)	−9.9(1.6)	−10.4(1.5)	−10.6(1.5)	−10.3(1.5)	−9.6(1.7)
n_{GS}	5/10	3/10	5/10	5/10	3/10	2/10

Table 3.

Run	$T_f = 50$ K	$T_f = 1$ K
1	−10.5	−11.7
2	−10.6	−8.6
3	−11.6	−12.1
4	−8.7	−8.8
5	−9.3	−7.4
6	−8.7	−8.9
7	−8.3	−12.1
8	−8.3	−12.2
9	−8.8	−7.1
10	−8.2	−7.5
11	−11.9	−9.9
12	−10.3	−7.3
13	−11.8	−8.4
14	−9.5	−10.6
15	−11.7	−10.3
16	−8.6	−12.2
17	−10.5	−12.2
18	−10.2	−9.1
19	−11.6	−11.9
20	−11.8	−12.1
$< E >$	−10.0(1.4)	−10.0(2.1)
n_{GS}	6/20	8/20

Table 4.

	Fixed sampling size			Dynamically changed sampling size	
Run	$\Delta E = 5$	$\Delta E = 10$	$\Delta E = 15$	$\Delta_m = 5$	$\Delta_m = 10$
1	−8.9	−11.9	−12.0	−10.4	−11.8
2	−10.1	−11.9	−11.6	−11.7	−11.8
3	−11.8	−10.5	−12.0	−11.6	−11.8
4	−10.6	−10.3	−11.8	−11.3	−11.3
5	−9.3	−10.3	−12.0	−11.9	−11.6
6	−7.6	−12.0	−11.9	−10.5	−11.8
7	−12.0	−11.8	−12.0	−11.6	−11.5
8	−12.0	−11.5	−11.5	−11.0	−11.6
9	−9.4	−10.8	−11.5	−11.9	−11.6
10	−9.6	−10.3	−11.8	−11.7	−11.8
$< E >$	−10.1(1.5)	−11.1(8)	−11.8(2)	−10.9(1.1)	−11.7(2)
n_{GS}	3/10	5/10	10/10	8/10	10/10

Table 5.

	Fixed sampling size	Dynamically changed sampling size
Run	$\Delta E = 15$	$\Delta_m = 10$
1	−11.6	−11.7
2	−12.0	−11.3
3	−10.2	−11.5
4	−10.1	−10.3
5	−11.9	−11.5
6	−12.0	−11.5
7	−11.9	−11.1
8	−11.7	−11.1
9	−11.8	−11.3
10	−11.9	−11.5
11	−12.0	−10.1
12	−12.1	−11.6
13	−12.0	−11.3
14	−11.8	−11.6
15	−11.3	−10.4
16	−11.9	−11.8
17	−12.0	−10.1
18	−11.9	−11.8
19	−11.9	−10.8
20	−11.6	−11.5
$< E >$	−11.7(6)	−11.2(6)
n_{GS}	18/20	15/20

Table 6.

ΔE	E_m	Type of structure
10	−10.5	B
11	−10.8	B
12	−10.5	B
13	−10.5	B
14	−10.6	B
15	−11.5	A

Figure Captions:

Fig. 1: Probability distribution $P(E)$ of the energy as a function of temperature T obtained by a regular multicanonical simulation with 1,000,000 MC sweeps.

Fig. 2a: Probability distribution of the energy for T = 300 K as obtained by a canonical simulation (*Cano*), a multicanonical simulation (*MuCa*) and simulated annealing (*SiAn*).

Fig. 2b: Probability distribution of the energy for T = 50 K as obtained by a canonical simulation (*Cano*), a multicanonical simulation (*MuCa*) and simulated annealing (*SiAn*).

Fig. 3: Average total energy $E_{tot} = E_{es} + E_{HB} + E_{vdW} + E_{tor}$ (+) and averages of its component terms, Coulomb energy E_{es} (X), hydrogen-bond energy E_{HB} ($\Diamond$), van der Waals energy E_{vdW} ($\Box$), and torsion energy E_{tor} ($\bigcirc$) as a function of temperature T. All values are calculated from a regular multicanonical simulation with 1,000,000 MC sweeps.

Fig. 4: Specific heat as a function of temperature T. The values are calculated from a regular multicanonical simulation with 1,000,000 MC sweeps.

Fig. 5: Average of the order parameter Op defined in Eq. (23) as a function of temperature T. The values are calculated from a regular multicanonical simulation with 1,000,000 MC sweeps.

Fig. 6: Probability distribution of the order parameter Op (defined in Eq. (23)) as a function of temperature T. The values are calculated from a regular multicanonical simulation with 1,000,000 MC sweeps.

Fig. 7: Fraction of groundstate-like configurations (*GS*), coil configurations (*COIL*), and intermediate configurations (*IM*) as a function of temperature T. A groundstate-like configuration differs no more than 20 degrees in at least 14 of the 19 dihedral angles from the groundstate; a coil configuration differs in at least 14 dihedral angles by more than 20 degrees from the groundstate configuration. The values are calculated from a regular multicanonical simulation with 1,000,000 MC sweeps.

Fig. 8: Enthalpy differences ΔH between groundstate-like configurations and coil configurations (+), between groundstate-like configurations and intermediate configurations ($\bigcirc$), and between intermediate configurations and coil configurations (X) as a function of temperature T. The values are calculated from a regular multicanonical simulation with 1,000,000 MC sweeps.

Fig. 9: Entropy differences $T\Delta S$ between groundstate-like configurations and coil configurations (+), between groundstate-like configurations and intermediate configurations ($\bigcirc$), and between intermediate configurations and coil configurations (X) as a function of temperature T. The values are calculated from a regular multicanonical simulation with 1,000,000 MC sweeps. The errors were smaller than the plot symbols.

Fig. 10: Free energy differences ΔG ($\triangle$), enthalpy differences ΔH (+) and entropy differences $T\Delta S$ ($\square$) between groundstate-like configurations and non-groundstate-like configurations as a function of temperature T. The values are calculated from a regular multicanonical simulation with 1,000,000 MC sweeps. The errors were smaller than the plot symbols.

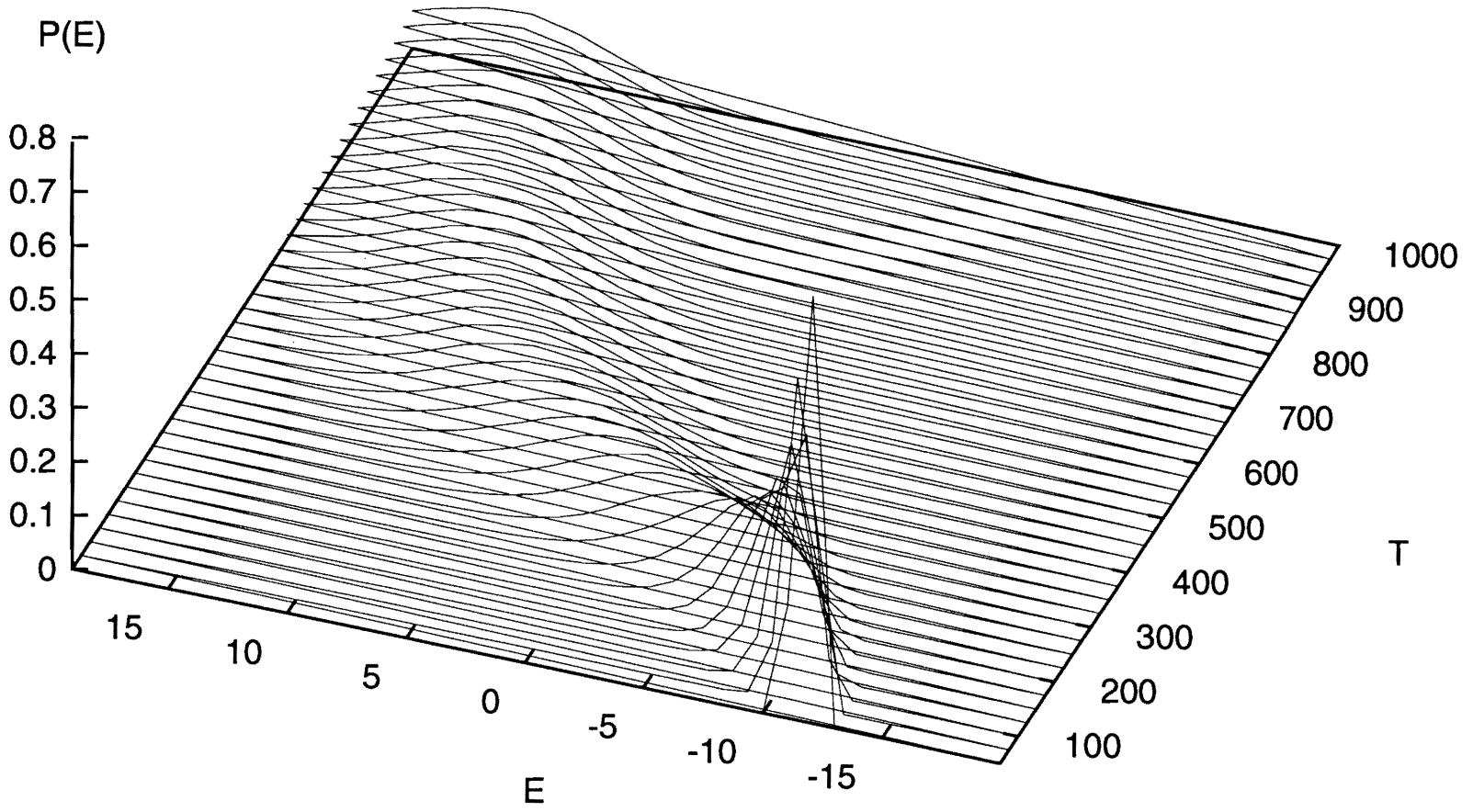
P(E)
0.8
0.7
0.6
0.5
0.4
0.3
0.2
0.1
0
15
10
5
0
-5
-10
-15
E
1000
900
800
700
600
500
400
300
200
100
T

Fig. 1

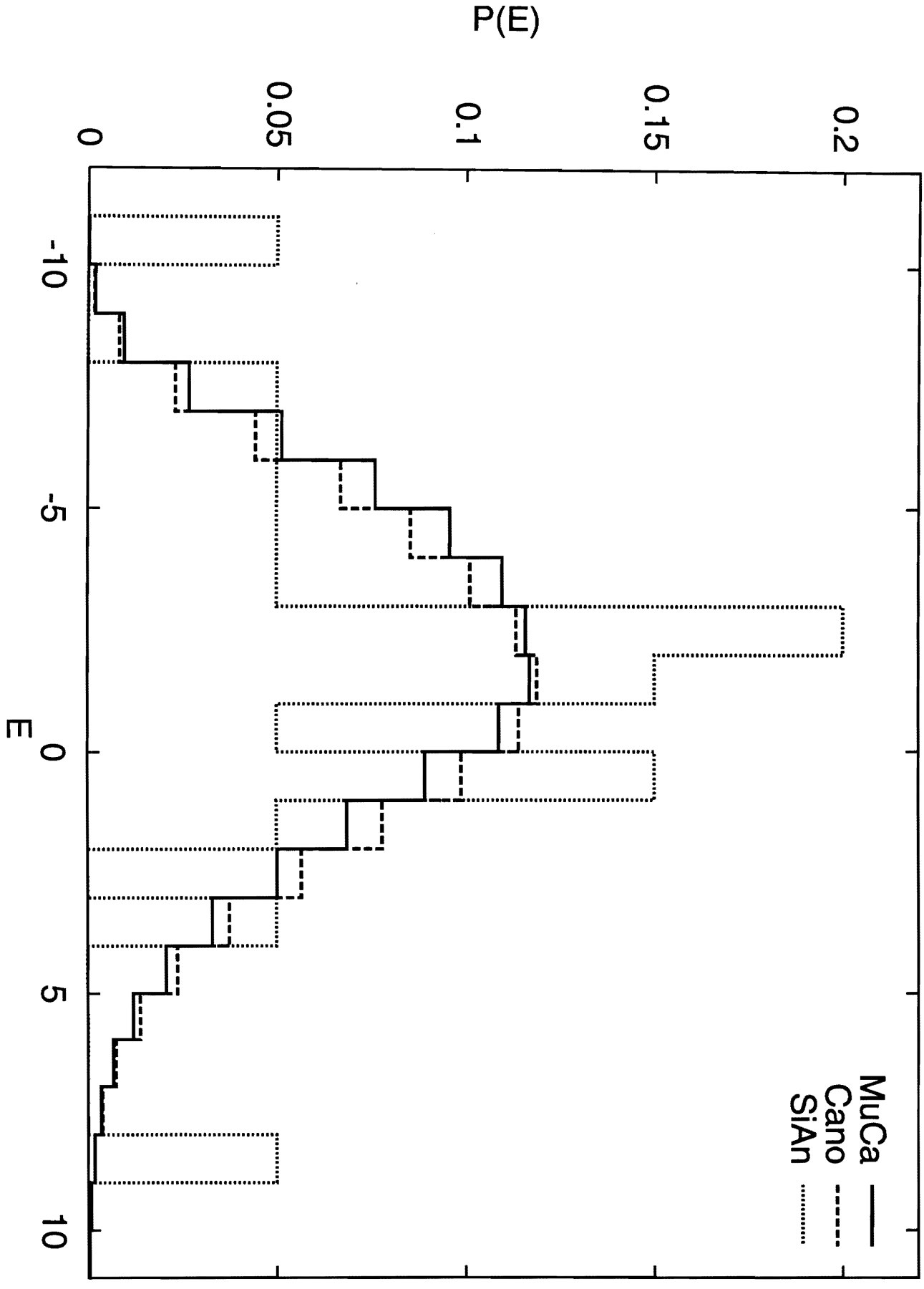

Fig. 2a

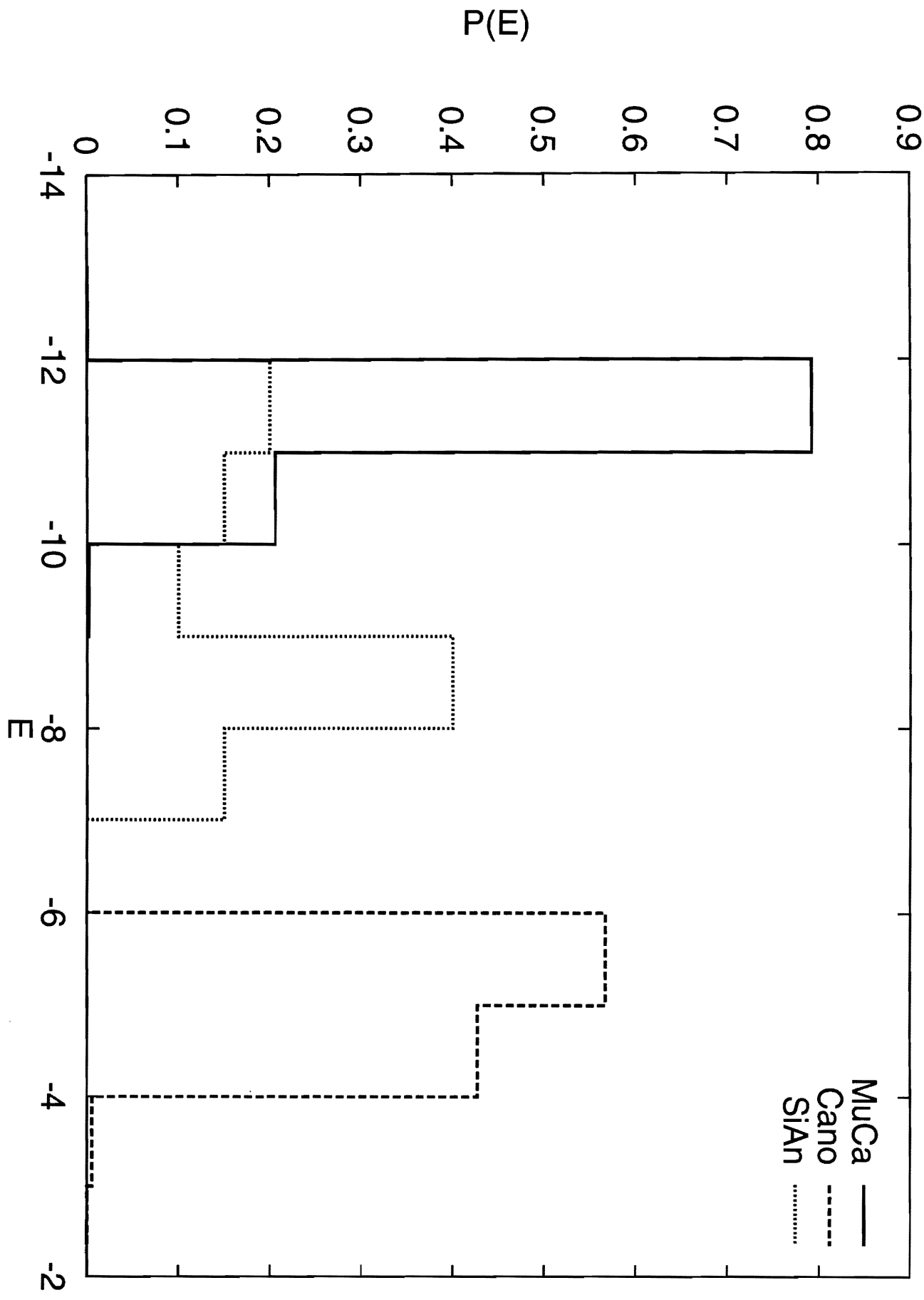

Fig. 2b

ENERGIES

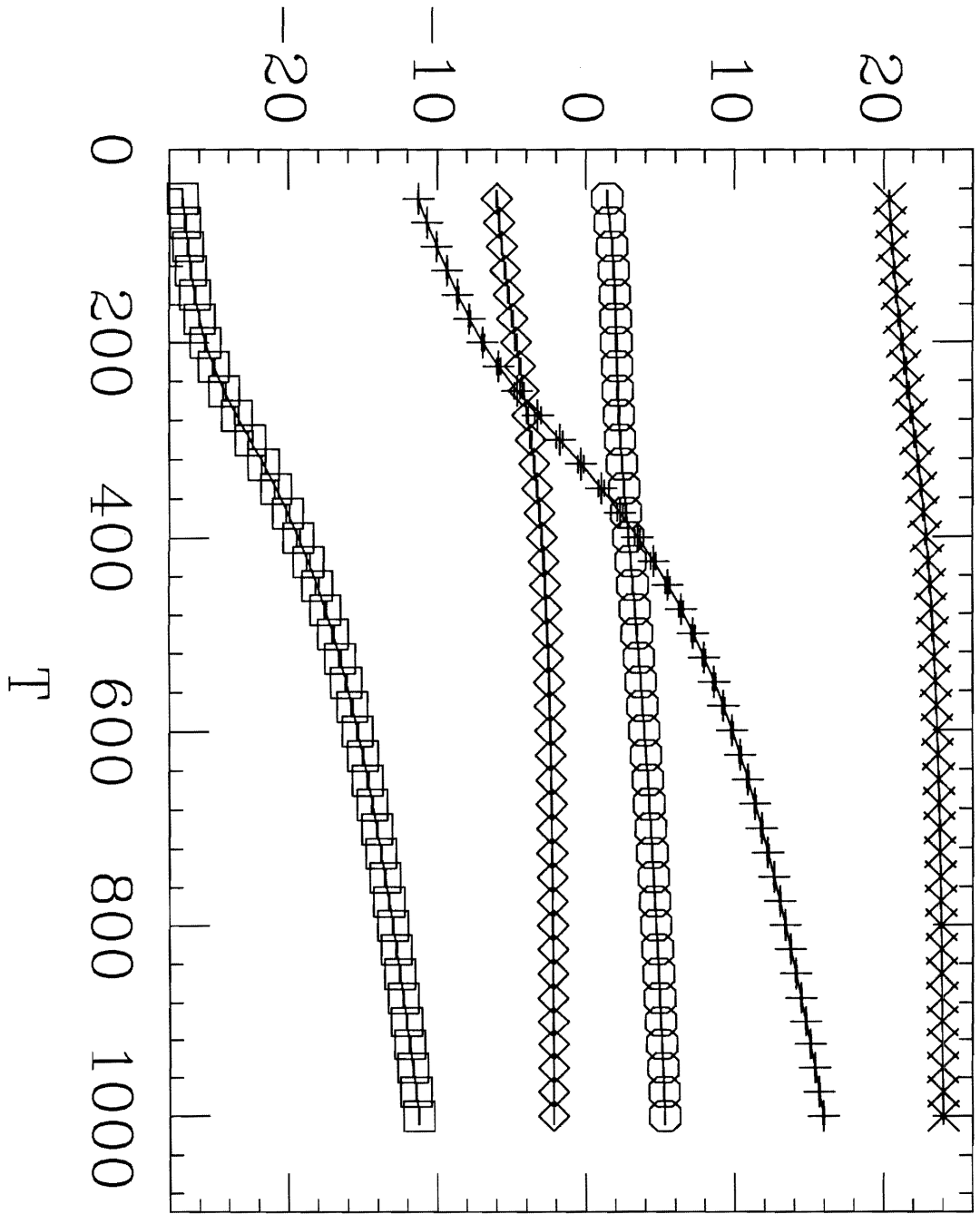

Fig. 3

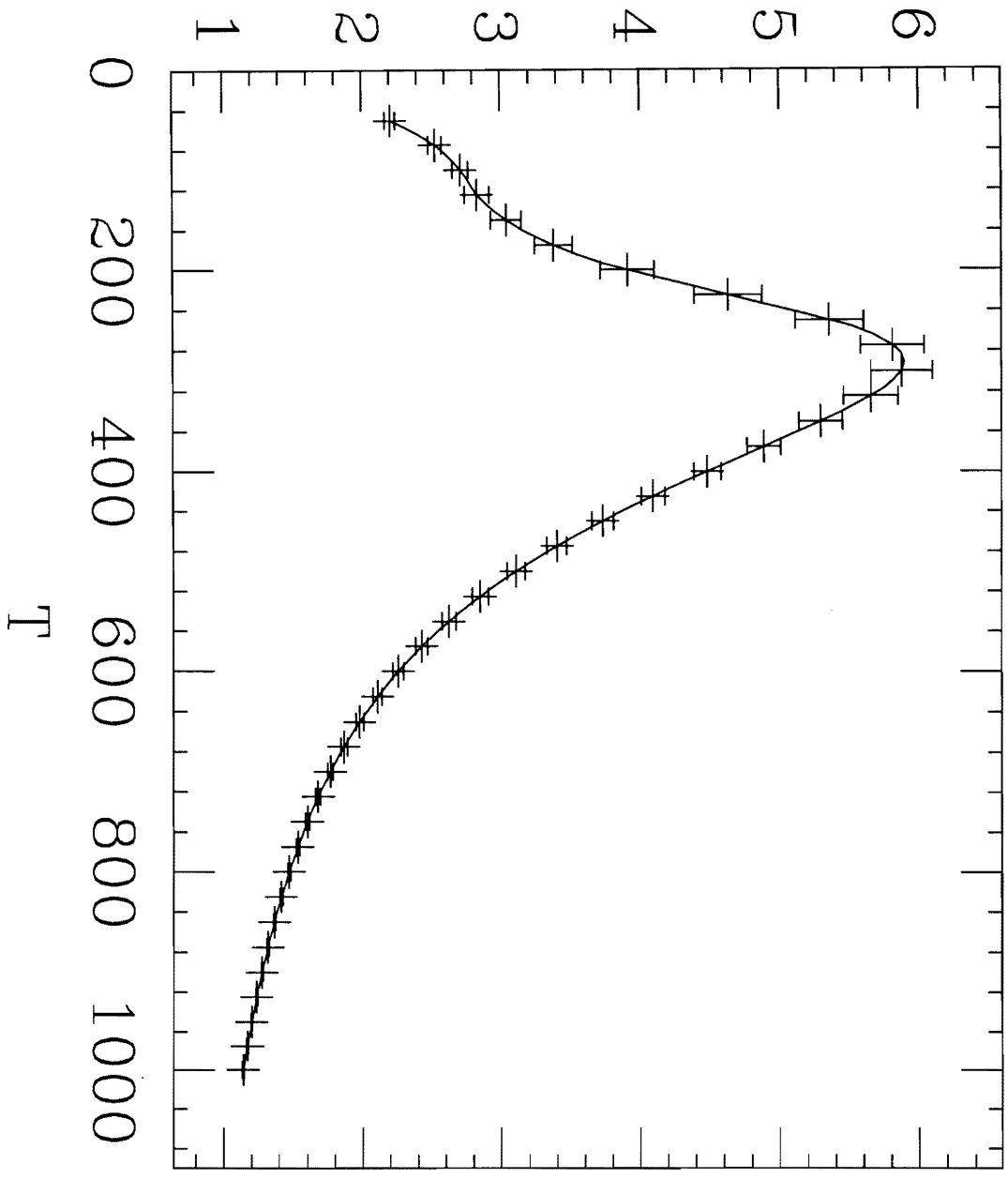

Fig. 4

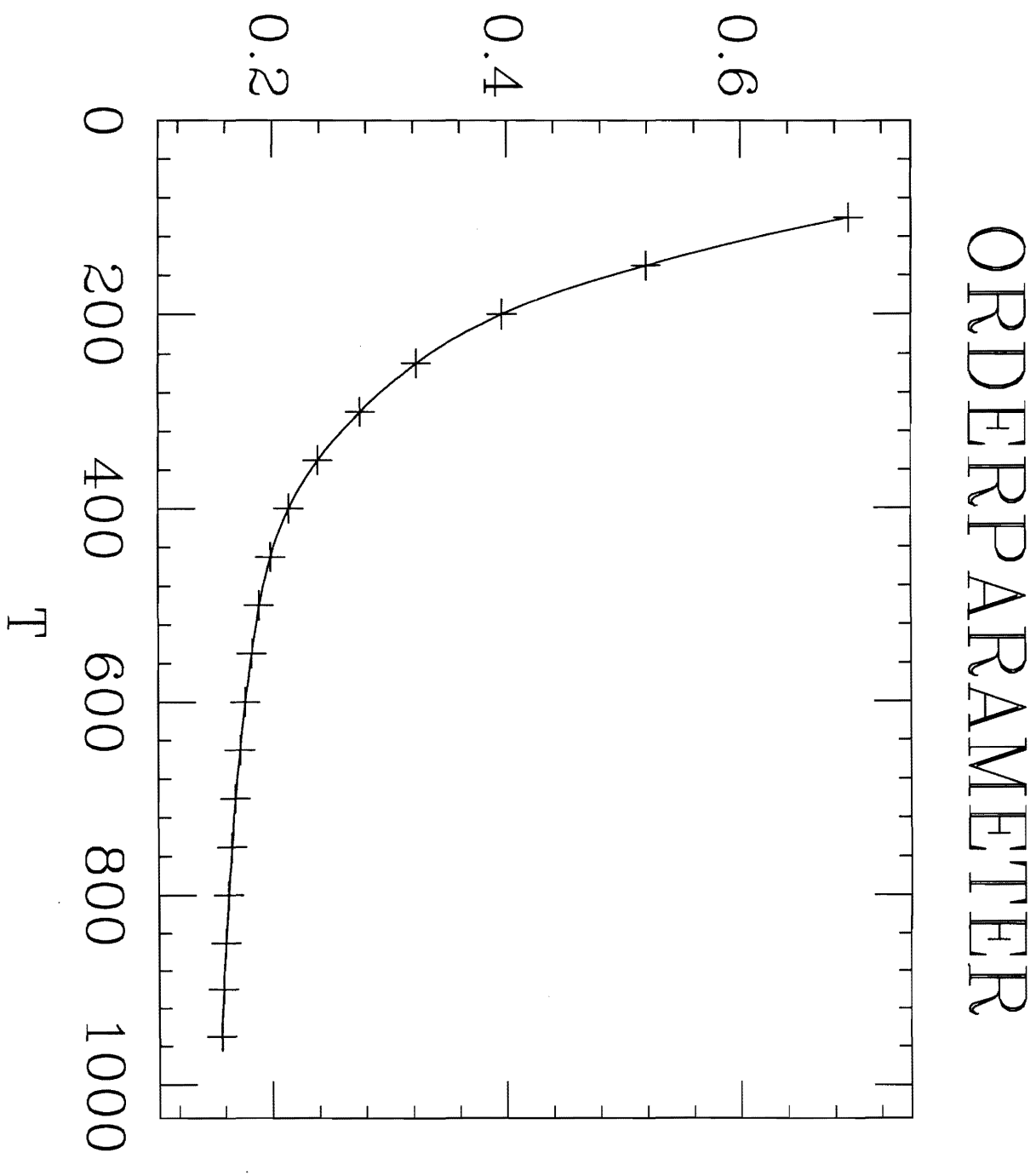

Fig. 5

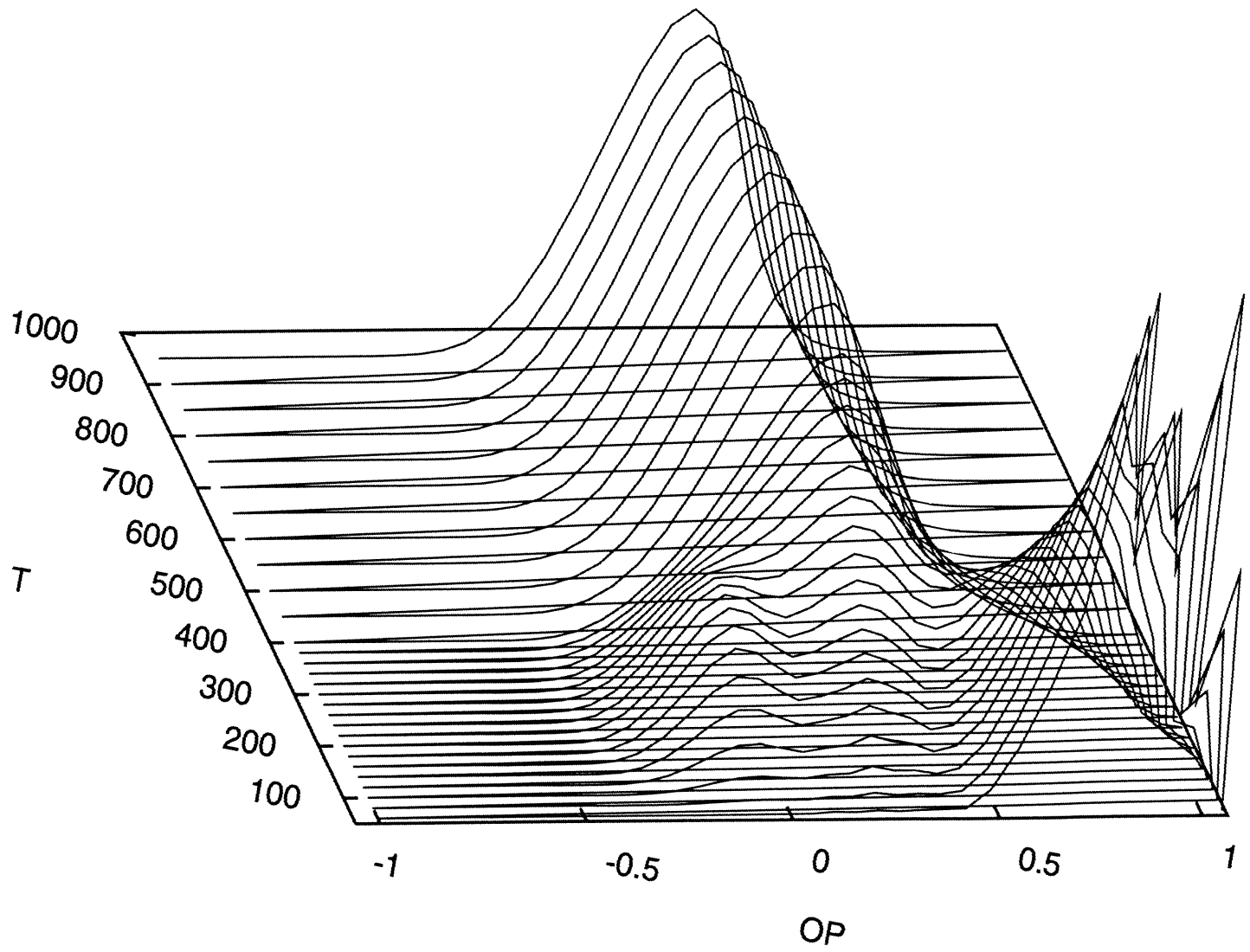

Fig. 6

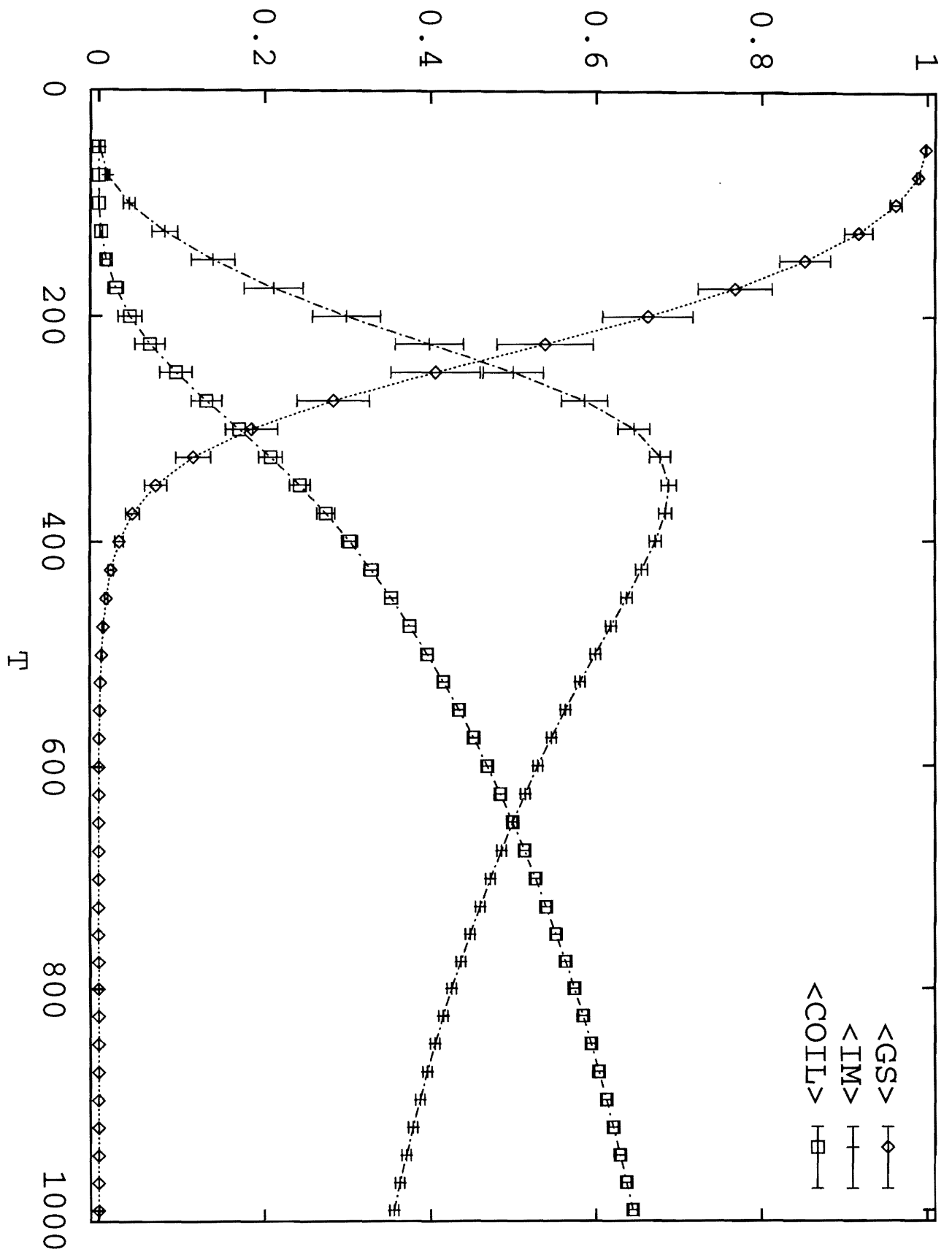
<% OF CONFIGURATIONS>
0
0.2
0.4
0.6
0.8
1
T
0
200
400
600
800
1000
<GS>
<IM>
<COIL>

Fig. 7

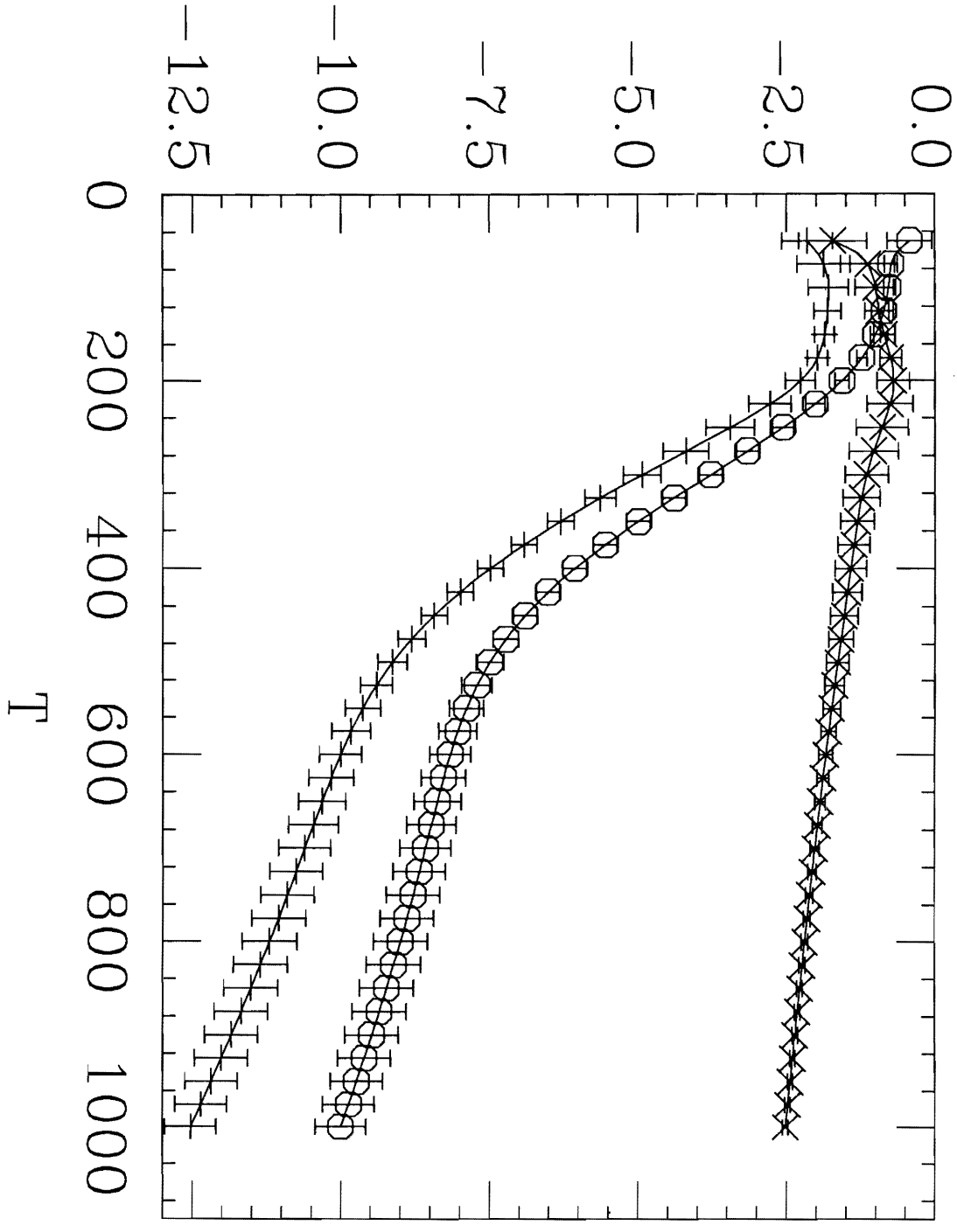

Fig. 8

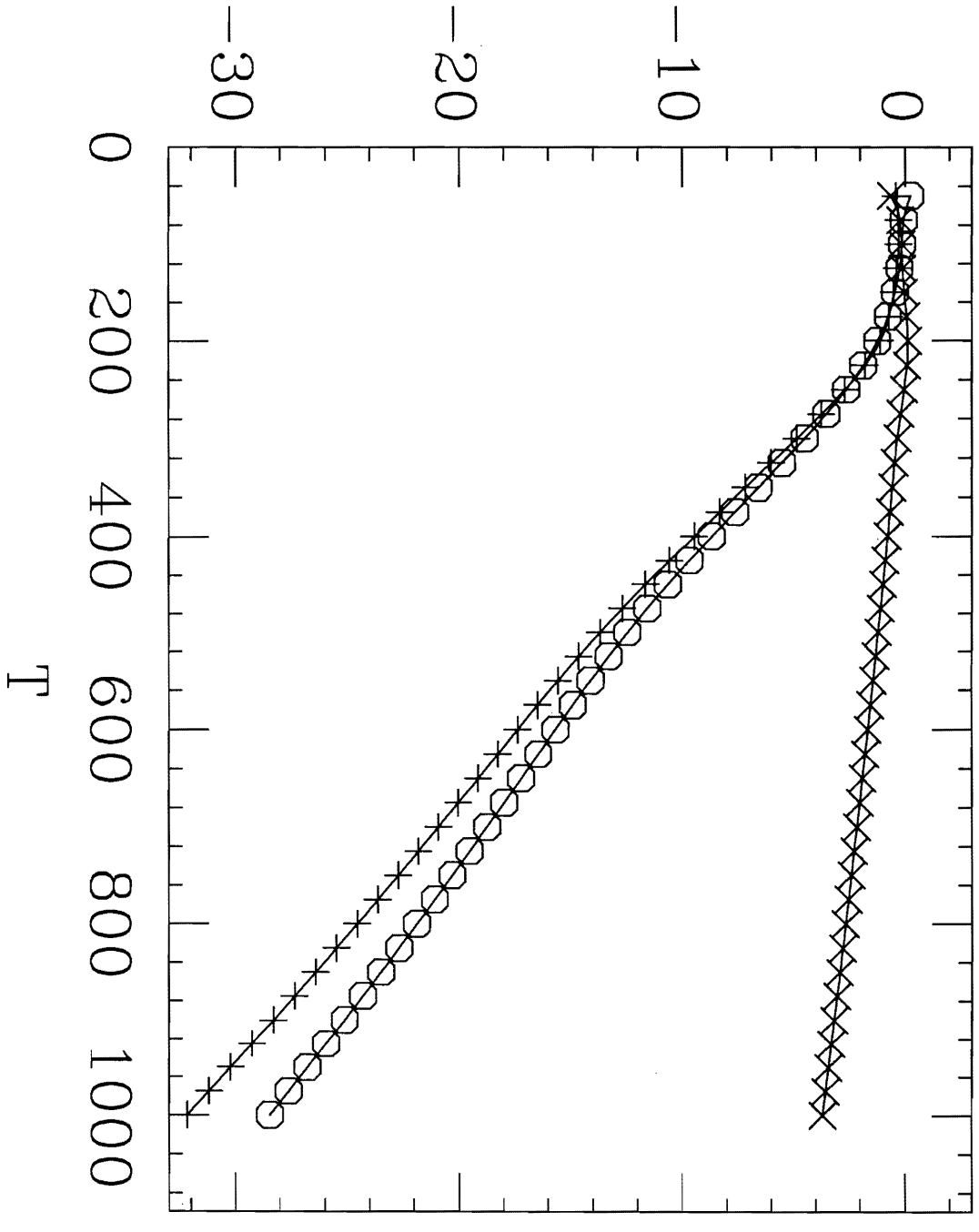

Fig. 9

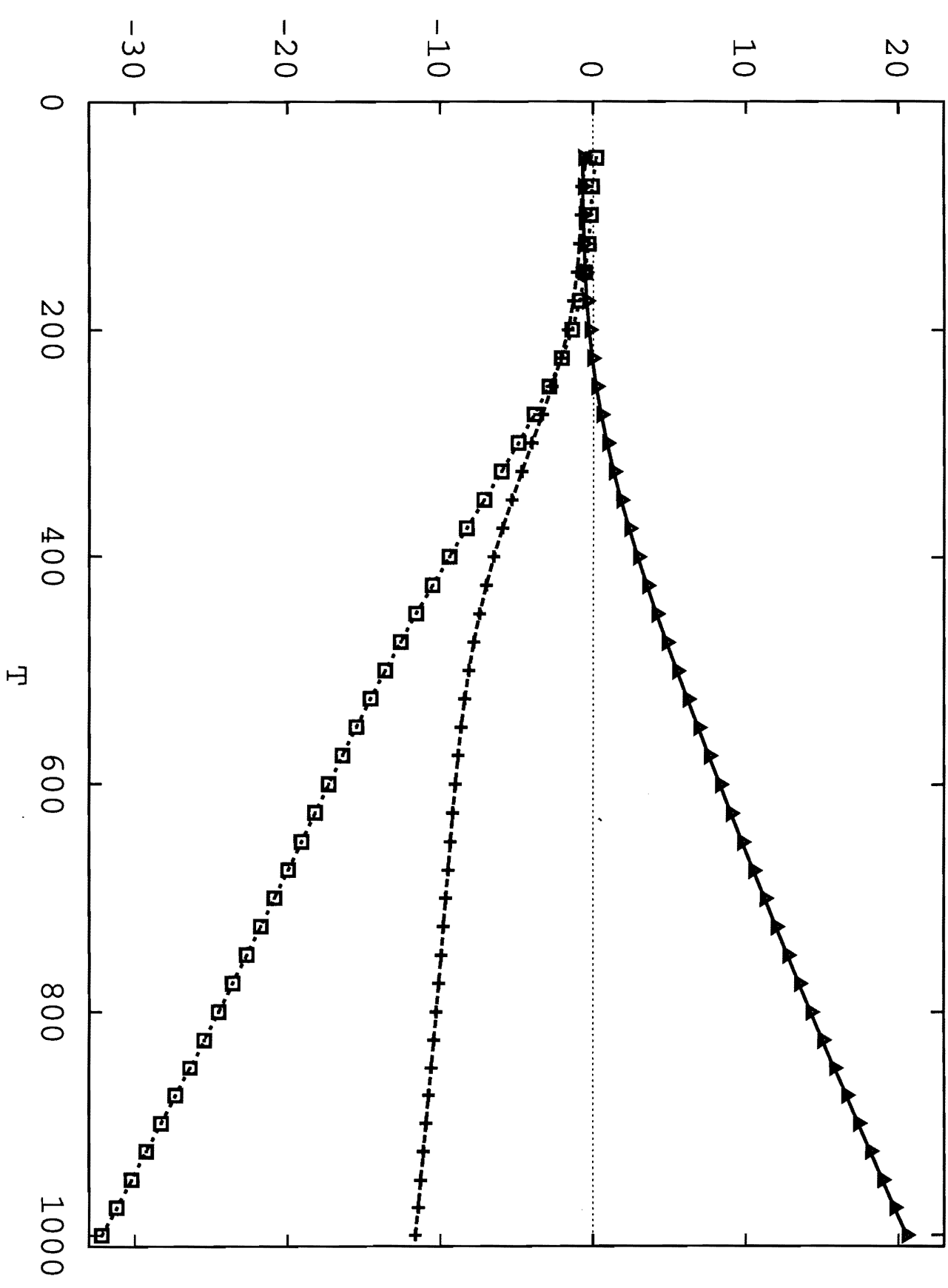

Fig. 10

Veröffentlichungen des Konrad-Zuse-Zentrum Berlin

SC 93- 2. M. Grötschel; A. Martin; R. Weismantel. *Packing Steiner Trees: Separation Algorithms.* *

SC 93- 3. Karin Gatermann; Bodo Werner. *Group Theoretical Mode Interactions with Different Symmetries.**

SC 93- 4. C. E. Ferreira; A. Martin; R. Weismantel. *Facets for the Multiple Knapsack Problem.**

SC 93- 5. Jürgen Richter-Gebert. *Mechanical Theorem Proving in Projective Geometry.*

SC-93- 6. Peter Deuflhard. *A Study of Lanczos-Type Iterations for Symmetric Indefinite Linear Systems.**

SC 93- 7. C. E. Ferreira; A. Martin; R. Weismantel. *A Cutting Plane Based Algorithm for the Multiple Knapsack Problem.**

SC 93- 8. Bodo Erdmann; Ronald H.W. Hoppe; Ralf Kornhuber. *LARGE Adaptive Multilevel - Methods for Obstacle Problems in Three Space Dimensions.**

SC 93- 9. M. Grötschel; C.L.Monma; M.Stoer. *Handbook in Operations Research and Management Science. Volume on "Networks". Chapter on "Design of Survivable Networks".**

SC 93-10. Christof Schütte. *A quasiresonant smoothing algorithm for the fast analysis of selective vibrational excitation.**

SC 93-11. Victor Reiner; Günter M. Ziegler. *Coxeter-associahedra.**

SC 93-12. J. Ackermann; R. Roitzsch. *On a Two–Dimensional Multilevel Adaptive Finite Element Method for the Time-Independent Schrödinger–Equation.**

SC 93-13. M. Grötschel; L. Lovasz. *Combinatorial Optimization.**

SC 93-14. Christof Schütte; Andreas Hohmann; Manfred Dinand. *Numerical Simulation of Relaxations Oscillations of Waveguide-Lasers.**

SC 93-15. A. Martin; R. Weismantel. *Packing Paths and Steiner Trees: Routing of Electronic Circuits.**

SC 93-16. K. Gatermann; B. Werner. *Secondary Hopf bifurcation caused by steady-state steady-state mode interaction.**

SC 93-17. Persi Diaconis; Bernd Sturmfels. *Algebraic Algorithms for Sampling from Conditional Distributions.**

SC 93-18. Ralf Kornhuber. *Monotone Multigrid Methods for Elliptic Variational Inequalities I.**

SC 93-19. Ralf Kornhuber. *Monotone Multigrid Methods for Elliptic Variational Inequalities II.**

SC 93-20. Mechthild Stoer; Geir Dahl. *A Polyhedral Approach to Multicommodity Survivable Network Design.**

SC 93-21. Ralf Kornhuber; Harry Yserentant. *Multilevel Methods for Elliptic Problems on Domains not Resolved by the Coarse Grid.**

SC 93-22. Peter Deuflhard; Jörg Ackermann. *Adaptive Discrete Galerkin-Methods for Macromolecular Processes.**

SC 93-23. Peter Deuflhard. *Cascadic Conjugate Gradient Methods for Elliptic Partial Differential Equations I. Algorithm and Numerical Results.**

SC 93-24. Frank Schmidt; Peter Deuflhard. *Discrete Transparent Boundary Conditions for the Numerical Solution of Fresnel's Equation.**

SC 93-25. Jürgen Richter-Gebert; Günter M. Ziegler *Huge Zonotopal Tilings and the Bohne-Dress Theorem**

SC 93-26. Martin Grötschel; Alexander Martin; Robert Weismantel. *Optimum Path Packing on Wheels: The Noncrossing Case.**

SC 93-27. Wolfram Koepf. *A package on formal power series.**Appeared in: The Mathematica Journal 4 (1994) 62-69

SC 93-28. R. Wunderling; H. Ch. Hege; M. Grammel. *On the Impact of Communication Latencies on Distributed Sparse LU Factorization.**

SC 93-29. Folkmar A. Bornemann; Bodo Erdmann; Ralf Kornhuber. *A Posteriori Error Estimates for Elliptic Problems.**

SC 93-31. Dominik Gruntz; Wolfram Koepf. *Formal Power Series.**

SC 93-32. Gerhard W. Zumbusch. *Symmetric Hierarchical Polynomials for the h-p-Version*

*of Finite Elements.**

SC 93-33. Folkmar A. Bornemann. *Interpolation Spaces and Optimal Multilevel Preconditioners.**

SC 93-34. Martin Grötschel and Manfred Padberg. *Ulysses 2000: In Search of Optimal Solutions to Hard Combinatorial Problems*

SC 93-35. Martin Seebass; Dennis Sullivan; Peter Wust; Peter Deuflhard; Roland Felix. *The Berlin Extension of the Stanford Hyperthermia Treatment Planning.**

SC 94- 1. Robert Weismantel. *On the 0/1 Knapsack Polytope.**

SC 94- 2. M. Grötschel; A. Martin; R. Weismantel. *The Steiner Tree Packing Problem in VLSI-Design.**

SC 94- 3. Jan Verschelde; Karin Gatermann. *Symmetric Newton Polytopes for Solving Sparse Polynomial Systems.**

SC 94- 4. Andreas Hohmann. *Object Oriented Design of Multilevel Newton and Continuation Methods.**

SC 94- 5. Wolfram Koepf. *Algorithmic Work with Orthogonal Polynomials and Special Functions.**

SC 94- 6. Svante Linusson. *Partitions with restricted block sizes, Möbius functions and the k-of-each problem.**

SC 94- 7. Bernd Gärtner; Günter M. Ziegler. *Randomized simplex algorithms on Klee-Minty cubes.**

SC 94- 8. Folkmar A. Bornemann. *On the Convergence of Cascadic Iterations for Elliptic Problem.**

SC 94- 9. Jens Lang. *Resolution Selfadaptive Computations on Chemical Reaction–Diffusion Problems with Internal Boundaries.**

SC 94-10. J. Ackermann; B. Erdmann; R. Roitzsch. *Adaptive Multilevel Finite Element Method for the Stationary Schrödinger Equation in Three Space Dimensions.**

SC 94-11. Karin Gatermann. *Semi-invariants, equivariants and algorithms.**

SC 94-12. Claudia Wulff; Andreas Hohmann; Peter Deuflhard. *Numerical Continuation of Periodic Orbits with Symmetry.**

SC 94-14. Atef Abdel-Aziz Abdel-Hamid; Ralf Borndörfer.*On the Complexity of Storage Assignment Problems.**

SC 94-15. Jochen Froehlich. *Parameter Derivatives of the Jacobi Polynomials and the Gaussian Hypergeometric Function.**

SC 94-19. Robert Weismantel. *Hilbert Bases and the Facets of Special Knapsack Polytopes.**

SC 94-20. Ulrich H.E. Hansmann; Yuko Okamoto.*Comparative Study of Multicanonical and Simulated Annealing Algorithms in the Protein Folding Problem.**

SC 94-21. Ulrich H.E. Hansmann.*Towards Ab Initio Prediction of Protein Conformations – The Multicanonical Approach.**

*available via anonymous-ftp: *ftp serv01.zib-berlin.de ... cd /pub get README*

Veröffentlichungen des Konrad-Zuse-Zentrum Berlin

TR 93- 1. J. Langendorf; O. Paetsch. *GRAZIL, Beschreibung der Version 6.1 des Plotpakets**

TR 93- 2. Herbert Melenk. *Algebraic Solution of Nonlinear Equation Systems in REDUCE.**

TR 93- 3. Ralf Borndörfer; Martin Grötschel; Fridolin Klostermeier; Christian Küttner. *Telebus-Disposition: Ein Konzept zur Serviceverbesserung bei gleichzeitiger Kostensenkung.*

TR 93- 4. Martin Grötschel; Joachim Lügger; Wolfgang Sperber. *Wissenschaftliches Publizieren und Elektronische Fachinformation im Umbruch: ein Situationsbericht aus der Sicht der Mathematik.**

TR 93- 5. Bodo Erdmann; Jens Lang; Rainer Roitzsch. *Kaskade Manual — Version 2.0.**

TR 93- 6. Günter M. Ziegler. *Lectures on Polytopes. (Preliminary Version.)* [out of print]

TR 93- 7. H. C. Hege; T. Höllerer; D. Stalling. *Volume Rendering. Mathematical Models and Algorithmic Aspects.**

TR 93- 8. Andreas Hohmann. *An Implementation of Extrapolation Codes in C++.**

TR 93- 9. Jens Lang. *KARDOS - KAskade Reaction Diffusion One-dimensional System.**

TR 93-10. Peter Deuflhard; Reinhard Bölling; Raoul H. Bott. *Materialien zur Euler-Vorlesung in Sanssouci.**

TR 93-12. Konrad Zuse. *Cellular structured space (Rechnender Raum) and physical phenomena.*

TR 93-13. Andreas Hohmann. *Inexact Gauss Newton Methods for Parameter Dependent Nonlinear Problems.**

TR 93-14. U. Nowak. *Adaptive Linienmethoden für nichtlineare parabolische Systeme.**

TR 94- 1. P. Deuflhard, H. C. Hege, E. Sedlmayr (eds.). *Scientific Computing in der Theoretischen Physik.**

TR 94- 2. Wolfram Koepf; Dieter Schmersau. *Spaces of Functions Satisfying Simple Differential Equations.**

TR 94- 3. Wolfram Koepf. *On Families of Iterated Derivatives.**

TR 94- 4. Christof Schütte. *A Quasiresonant Smoothing Algorithm for Solving Large Highly Oscillatory Differential Equations from Quantum Chemistry.**

TR 94- 5. Gerhard W. Zumbusch. *Visualizing Functions of the h-p-Version of Finite Elements.**

TR 94- 6. Herbert Melenk. *The Complexity Barrier in REDUCE - a Case Study.**

TR 94- 7. W. Dalitz, M. Grötschel, J. Lügger, W. Sperber. *Neue Perspektiven eines verteilten Informationssystems für die Mathematik.**

TR 94- 8. W. Dalitz, M. Grötschel, J. Lügger, W. Sperber. *New Perspectives of a Distributed Information System for Mathematics.**

*available via anonymous-ftp: *ftp serv01.zib-berlin.de ... cd /pub get README*